The Matter Power Spectrum of Dark Energy Models and the Harrison-Zel'dovich Prescription

Ivan Duran [a],[1] Fernando Atrio-Barandela[b],[2] and Diego Pavón[c1]

[1] *Departamento de Física, Universidad Autónoma de Barcelona, Barcelona, Spain*

[2] *Departamento de Física Fundamental, Universidad de Salamanca, Spain*

According to the Harrison-Zel'dovich prescription, the amplitude of matter density perturbations at horizon crossing is the same at all scales. Based on this prescription, we show how to construct the matter power spectrum of generic dark energy models from the power spectrum of a ΛCDM model without the need of solving in full the dynamical equations describing the evolution of all energy density perturbations. Our approach allows to make model predictions of observables that can be expressed in terms of the matter power spectrum alone, such as the amplitude of matter fluctuations, peculiar velocities, cosmic microwave background temperature anisotropies on large angular scales or the weak lensing convergence spectrum. Then, models that have been tested only at the background level using the rate of the expansion of the Universe can now be tested using data on gravitational clustering and on large scale structure. This method can save a lot of effort in checking the validity of dark energy models. As an example of the accurateness of the approximation used, we compute the power spectrum of different dark energy models with constant equation of state parameter ($w_{DE} = -0.1$, -0.5 and -0.8, ruled out by observations but easy to compare to numerical solutions) using our methodology and discuss the constraints imposed by the low multipoles of the cosmic microwave background.

[a] E-mail address: ivan.duran@uab.es
[b] E-mail address: atrio@usal.es
[c] E-mail address: diego.pavon@uab.es

I. INTRODUCTION

In the concordance ΛCDM cosmological model, the current accelerated phase of expansion is driven by a cosmological constant Λ that dominates the present energy density of the Universe, whose equation of state (EoS) parameter is $w = -1$. The second component in importance is cold dark matter (DM), a non-baryonic dust component that drives the growth of large scale structure (LSS). This simple model fits rather well the observational data and requires the minimum set of cosmological parameters [1]. Also, it is the preferred model based on statistical selection criteria [2]. The observational successes of the ΛCDM cosmology is linked to its capacity to reproduce the right sequence of cosmological eras: matter-radiation equality occurs well before recombination and the matter dominated period lasts long enough to allow the growth of LSS. The length of the radiation and matter periods are crucial to determine the shape of the matter and radiation power spectra. Alternative models must also reproduce the correct sequence of cosmological eras to fit the data [3].

While the ΛCDM model fits the observational data very well, it appears rather unsatisfactory from the theoretical point of view. In fact, a cosmological constant is not very appealing. Its measured value is 120 orders of magnitude smaller than the expected amplitude at the Planck scale [4] and introduces the so-called coincidence problem (i.e., "why are the densities of DM and dark energy (DE) of the same order precisely today?") [5]. This is why a plethora of more flexible models that behave akin to the ΛCDM at the background level have been introduced over the years -see [6] for recent reviews. This complicates enormously the task of judiciously deciding which model should be preferred over all the others in view of their observational and theoretical merits. For instance, the acceleration could be driven by a dark energy component with EoS parameter $w_{DE} \neq -1$ [7], constant or variable on cosmological timescales. The simplest variants require cosmological parameters to be fine tuned at some initial time, suffering also -though, at a lower extent- from the coincidence problem and more complex models have been introduced [8]. Before carrying out a detailed analysis, these alternatives first use probes of the cosmic expansion history such as luminosity distances derived from supernovae type Ia data, angular diameter distances from baryon acoustic oscillations (BAO), the expansion rate, H, at various redshifts, etc. [9, 10]. Data on matter density perturbations and cosmic microwave background (CMB) anisotropies provide stronger constraints but require to solve the time evolution of the density perturbations in all components. In general, the resulting set of equations is far more involved than in the standard ΛCDM model. Furthermore, small differences on the dynamics of the dark sector change the equations governing the evolution of matter perturbations [11], and no generic constraints can be imposed on large classes of models. As a result, many models in the literature have not been constrained by the current data on density inhomogeneities and CMB temperature anisotropies -see e.g. [12].

The aim of this paper is to show how to derive the matter power spectrum of a generic DE model without the need of solving in full the perturbation equations for the radiation and matter components. Several observables can be computed in terms of the matter power spectrum alone and can be used to constrain the model beyond the expansion rate. The observables include: (a) the fluctuation of the matter density perturbations on a sphere of $8h^{-1}$Mpc, σ_8 [13]; (b) the rms peculiar velocity of matter on spheres of radius R, $\langle v^2(R)\rangle^{1/2}$ [14]; (c) the weak lensing convergence spectrum [15]; (d) the Sachs-Wolfe (SW) and Integrated Sachs-Wolfe (ISW) components of the CMB temperature anisotropies [16]; (e) the cross-correlation of the ISW with templates of projected density of galaxies [17], etc. For example, the SW and ISW effects are the dominant contributions to the CMB anisotropies at low multipoles. If the power spectrum is normalized to the measured value $\sigma_8 = 0.801 \pm 0.030$ [18], the predicted low order multipoles of the CMB, the peculiar velocity on a given scale [19] or the measured ISW-Large Scale Structure cross-correlation [20] can be compared with observations. Our method provides simple tests of models using a wealth of data beyond luminosity and angular diameter distance measurements.

The idea of how to construct the matter power spectrum is based on the Harrison-Zel'dovich (HZ) [21] prescription. For any two models, the amplitude of density perturbations are specified at horizon crossing instead of at some arbitrary initial hypersurface. The final spectrum will differ only by the subsequent (subhorizon) evolution of each single mode. If we use as a starting model one that is implemented on publicly available numerical codes like CMBFAST [22], for example the concordance ΛCDM model, we will be able to construct the power spectrum of a generic DE model (not implemented on numerical codes). The method can be used to derive the power spectrum ranging from galaxy to horizon scales, i.e., at all the scales that can be observed at present.

In developing this method, our aim is not to use it to solve models of DE with a constant EoS parameter.

In section III, we consider a DE model with constant EoS parameter, $w = -0.5$ (though being aware that it is observationally discarded) just to illustrate the accurateness of the method in a model which, on the one hand, it is easy to obtain the exact evolution of the perturbations and, on the other hand, its evolution differs substantially from that of the standard ΛCDM. With this we can see that obtaining the matter power spectrum of a DE model from the one of ΛCDM is reasonable also in cases when both models differ greatly at the background level.

This method can be useful in solving the perturbation equations of interacting DE-DM models [10, 23–25]. Many of these models aim to describe the Universe at low redshifts, when DM and DE dominate the expansion. Following our method, the matter perturbations evolve as in the ΛCDM model before horizon crossing (this avoids the need of explicitly introducing initial conditions for the perturbations). Moreover, because it suffices to compute the evolution of the perturbations of the particular DE model considered after they enter the horizon, the set of equations to be solved gets greatly simplified. This is shown in section III.

Briefly, section II recalls the basics of the HZ prescription. Section III describes how the matter power spectrum of a generic DE model can be constructed. Section IV discusses how to calculate the low multipoles on CMB temperature anisotropies to constrain the model. Finally, Section V summarizes the main results of the paper.

II. THE HARRISON-ZELDOVICH PRESCRIPTION

In their seminal papers, Harrison and Zel'dovich [21] computed the present matter power spectrum assuming that all perturbations at horizon crossing have the same amplitude. Then, they computed the matter power spectrum $P(k)$ at the present time after accounting for the subhorizon evolution of each mode. To illustrate their argument, let us construct the power spectrum of the standard CDM model, a model that only contains DM, baryons and radiation (subscripts c, b, and r, respectively), and verifies $\Omega_c+\Omega_b+\Omega_r = 1$, where Ω_i is the energy density of component i in units of the critical density. Let us define the density contrast by $\delta(k,t) = (\delta\rho/\bar{\rho})(k,t)$. In the linear regime, spatial and time dependence can be separated: $\delta(k,t) = \delta(k)D_+(t)/D_+(t_0)$, where $D_+(t)$ denotes the growing solution and $\delta(k)$ is evaluated at the present time, t_0. The current power spectrum is then defined as: $P(k) = |\delta(k)|^2$.

In the standard cold dark matter (CDM) model, $D_+(t) \approx$ const during the radiation dominated era and $D_+(t) = D_+(t_{in})(t/t_{in})^{2/3}$, during the matter dominated period. The HZ prescription establishes that all mass perturbations, defined as $\Delta(k,t) = \frac{1}{2\pi^2}k^3P(k)(D_+(t)/D_+(t_0))^2$, have the same amplitude at the time t_{in} when they enter the horizon, i.e., $a(t_{in})\lambda_{in} = d_H(t_{in})$ where $a(t)$ is the scale factor, $d_H(t)$ the radius of the horizon, and λ_{in} the comoving wavelength of each particular mode; $k_{in} = 2\pi/\lambda_{in}$ would be the corresponding wavenumber. In particular

$$\Delta(k_{in}, t_{in}) = \text{const} = \Delta(k_{eq}, t_{eq}), \tag{1}$$

with t_{eq} the moment of matter-radiation equality.

Once a perturbation enters the horizon, it will evolve as $D_+(t)$ and we can write

$$\Delta(k_{eq}, t_0) = \left(\frac{D_+(t_0)}{D_+(t_{eq})}\right)^2 \Delta(k_{eq}, t_{eq}) = \left(\frac{D_+(t_0)}{D_+(t_{eq})}\right)^2 \Delta(k_{in}, t_{in}) = \left(\frac{D_+(t_{in})}{D_+(t_{eq})}\right)^2 \Delta(k_{in}, t_0). \tag{2}$$

The evolution after horizon crossing depends on whether it occurs before or after matter-radiation equality:

1. If $t_{in} < t_{eq}$, then $D_+(t_{in}) = D_+(t_{eq})$ because perturbations are essentially frozen in the radiation era. Consequently, $P(k_{in}) = P(k_{eq})\,(k_{in}/k_{eq})^{-3}$.

2. If $t_{in} > t_{eq}$, then $D_+(t_{in})/D_+(t_{eq}) = (t_{in}/t_{eq})^{2/3} = (k_{eq}/k_{in})^2$. In the last equality we have used the relation between the comoving wavenumber and the time of horizon crossing $k_{in} \propto t_{in}^{-1/3}$, valid in the matter era. Then $P(k_{in}) = P(k_{eq})\,(k_{in}/k_{eq})$.

As a consequence of the growth of density perturbations in the matter and radiation epochs, the power spectrum has two asymptotic regimes: $P(k) \sim k^1, k^{-3}$ at large and small scales, respectively, with a maximum at the scale of matter-radiation equality. Since the transition from the radiation to the matter dominated period is not instantaneous, $P(k)$ has a smooth maximum about matter-radiation equality, at k_{eq}. The power spectrum is conveniently expressed as $P(k) = A\, k^n\, T^2(k)$, where A is a normalization constant and n the spectral index at large scales. The transfer function $T(k)$ is determined by the growth rate within the horizon. In the specific case of the HZ prediction, $n = 1$.

III. THE MATTER POWER SPECTRUM OF GENERIC DARK ENERGY MODELS

The spectra of the concordance ΛCDM models differ from the spectra of models with no cosmological constant in two main respects, namely: (1) the scale of matter radiation equality is shifted to larger scales, and (2) the growth factor of matter density perturbations slows down once the overall expansion accelerates. As mentioned above, in this section we shall show how to compute the present matter power spectrum of a DE model, in principle not implemented on a numerical package, from the power spectrum of a model that is implemented. As an example, we shall construct the power spectrum of models with $w_{DE} = -0.8, -0.5, -0.1$ from the concordance ΛCDM. The evolution of density perturbations of DE models with constant EoS is implemented in standard packages like CMBFAST and can be computed numerically but they will be useful to estimate the accuracy of the method. For simplicity, all models will share identical cosmological parameters, namely $\Omega_\Lambda = 0.73, \Omega_{DM} = 0.23, \Omega_b = 0.04$, $H_0 = 71$ km/s/Mpc and $n = 1$. The models differ only in the EoS parameter, w_{DE}.

Following the HZ prescription, we assume that all perturbations have the same amplitude at horizon crossing. Then, we just need to compare the growth rate of density perturbations in both models once perturbations cross the horizon. Even if the subhorizon evolution of density perturbations is the same in the ΛCDM as in the DE model, the final power spectrum could be different. In each model, fixed comoving wavelengths λ_{in} cross the horizon at different times t_{in} and the growth rate from t_{in} to the present time t_0 will be different for each of them. Then, we need to determine: (1) the size of the horizon as a function of time to fix when a perturbation crosses the horizon, and (2) solve the equations of evolution of subhorizon density perturbations during the radiation, matter and accelerated expansion epochs. If DM and DE density perturbations evolve independently during the radiation regime, we can expect the evolution of DM perturbations to be independent of the model. Specifically, in the radiation era the expansion timescale is $t_{exp} \propto (G\rho_{rad})^{-1/2}$ while if the free-fall time of matter within a density perturbation is $t_{ff} \propto (G\rho_m)^{-1/2}$, much smaller than the expansion timescale and matter perturbations will not grow significantly during the radiation regime. With this simplifying assumption, if the DE model and ΛCDM have the same matter-radiation equality and perturbations cross the horizon at the same time, then the power spectrum at small scales will have the same shape in both models. Without restricting the applicability of our method, this assumption guarantees that the DE model will pass the constraints imposed by the galaxy distribution on scales $\lambda \leq 100\mathrm{Mpc}/h$ not less well than the ΛCDM model.

Our method is more easily implemented when the equations of evolution of subhorizon sized perturbations after matter-radiation equality form a closed system and can be solved independently for each energy density component (see [26] for extensive reviews on cosmological perturbation theory). If both models have identical evolution during the radiation era, once the Universe becomes matter dominated the anisotropic stress due to neutrinos will be negligible and, in the Newtonian gauge, it will suffice just one single gravitational potential, say ϕ, to determine the flat metric element

$$ds^2 = -(1+2\phi)dt^2 + a^2(1-2\phi)dx^i dx_i\,. \tag{3}$$

From the (0,0) component of Einstein's equations, the evolution of the gravitational potential is given by

$$\frac{k^2}{a^2}\phi + 3H\left(\dot{\phi} + H\phi\right) = -4\pi G \sum \bar{\rho}_i \delta_i\,, \tag{4}$$

where the sum extends over all matter components. If the energy components interact only gravitationally between themselves, then the energy-momentum tensors are individually conserved. For a generic component

A, by perturbing the conservation equation $T_A^{\mu\nu}{}_{;\mu} = 0$ one obtains

$$\dot{\delta}_A = -(1+w_A)\left(\frac{\theta_A}{a} - 3\dot{\phi}\right) - 3H\left(c_{s,A}^2 - w_A\right)\delta_A, \tag{5}$$

$$\dot{\theta}_A = -H(1-3w_A)\theta_A - \frac{\dot{w}_A}{1+w_A}\theta_A + \frac{k^2}{a\,(1+w_A)}c_{s,A}^2\delta_A + \frac{k^2}{a}\phi, \tag{6}$$

where $c_{s,A}^2 = \frac{\delta P_A}{\delta \rho_A}$ is the sound speed, $\theta_A = k^2 v_A$, and v_A is the velocity field. For a more general treatment, including interaction between DE and DM, see e.g. [27]. When the evolution is subhorizon, $k \gg aH$ and time derivatives can be neglected compared to spatial gradients, eq. (4) reduces to the Poisson equation:

$$k^2\phi = -4\pi G a^2 \sum \rho_i \delta_i \,. \tag{7}$$

Equations (5) and (6) can be specialized to the case of DM, baryons and DE, $w_c = w_b = c_{s,c} = c_{s,b} = 0$. If the DE sound speed is $c_{s,DE} = 1$, then it will not cluster at small scales and we can take $\delta_{DE} \approx 0$. Under this assumption, the equations of evolution of matter density perturbations, defined as $\bar{\rho}_m\delta_m = \bar{\rho}_c\delta_c + \bar{\rho}_b\delta_b$ are:

$$\dot{\delta}_m = \frac{\theta_m}{a}, \tag{8}$$

$$\dot{\theta}_m = -H\theta_m - \frac{k^2\phi}{a}, \tag{9}$$

$$k^2\phi = -4\pi G a^2 \bar{\rho}_m \delta_m. \tag{10}$$

From this equations, the evolution of matter density perturbations is described by a single second order differential equation:

$$\ddot{\delta}_m + 2H\dot{\delta}_m - 4\pi G\bar{\rho}_m\delta_m = 0. \tag{11}$$

This equation does not depend on unknown functions, so the evolution of matter density perturbations can be solved exactly, as required by our method. In terms of the growth function $f \equiv \frac{d\ln\delta_m}{d\ln a}$, Eq. (11) could be transformed into an even simpler, first order, differential equation (see e.g. [10, 28]).

Let $D_+(t)$ be the growing mode solution of Eq. (11). To solve the equation, we need to specify the initial conditions at some arbitrary time. In the CMBFAST code, this is done at some initial space-like hypersurface. In HZ, all modes have the same amplitude at horizon crossing, i.e., amplitudes are fixed at different times for different modes. This amplitude will depend on the model, but for the same wavelength the ratio of amplitudes of different models will be constant, independent of scale, and this factor could be absorbed into the normalization. But even if the amplitudes at horizon crossing were the same, the current amplitudes will differ because of their different growth rates. When a perturbation of a fixed scale k_{in} enters the horizon at time $t_{in,DE}$ and $t_{in,\Lambda CDM}$ it grows by a factor $D_{+,DE}(t_{0,DE})/D_{+,DE}(t_{in,DE})$ and $D_{+,\Lambda CDM}(t_{0,\Lambda CDM})/D_{+,\Lambda CDM}(t_{in,\Lambda CDM})$, respectively. Therefore, the final amplitudes will differ by a factor

$$Q(k_{in}) = \frac{D_{+,DE}(t_{0,DE})/D_{+,DE}(t_{in,DE})}{D_{+,\Lambda CDM}(t_{0,\Lambda CDM})/D_{+,\Lambda CDM}(t_{in,\Lambda CDM})}\,. \tag{12}$$

As a result,

$$P_{DE}(k) = Q^2(k) P_{\Lambda CDM}(k). \tag{13}$$

This identity holds even if the spectral index differs from unity, $n \neq 1$.

To derive $Q(k)$ for each cosmological model we first compute the horizon radius, $d_H(z)$, to determine when a mode enters the horizon, and then solve the dynamical equations to find the subhorizon growth factor $D_+(z)$ after matter-radiation equality. If subhorizon perturbations in ΛCDM and DE models grow at the same rate in the radiation dominated regime, then $Q(k) = \text{const}$ and $\sigma_{8,DE} = Q(2\pi/8h^{-1}Mpc)\sigma_{8,\Lambda CDM}$. If both power

spectra are normalized at the same amplitude at small scales, then $Q(k \gg k_{eq}) = 1$ and DE and ΛCDM spectra will coincide at small scales. The method could be applied to superhorizon scales if the equations of evolution formed a closed system. If not, one can simply extrapolate their amplitude using the HZ prescription. If required, it could also be generalized to include perturbations in other components such as DE. It suffices to specify the amplitude of every component at horizon crossing and follow its subsequent evolution.

In Figure 1a, we plot the ratio of the comoving size of the horizon between different models; the thick solid (red) and dashed (blue) lines correspond to the ratio of the horizon size of the $w_{DE} = -0.5$ DE and ΛCDM models with respect to the standard ($\Omega_\Lambda = 0$, $\Omega_m = 1$) CDM model. As expected, the size of the horizon is the same in the radiation dominated regime irrespective of the cosmology. The thin (black) solid line represents the ratio of the ΛCDM horizon size to that of the $w_{DE} = -0.5$ DE model, i.e., $d_{H,\Lambda CDM}/d_{H,DE}$. In this case the ratio is very similar up to $z \approx 30$. The difference arises because the period of accelerated expansion starts earlier in the DE model. In Figure 1b we plot the growth factor (in units of the standard CDM growth factor) of the $w_{DE} = -0.5$ DE model, solid (red) line, and the concordance ΛCDM model, dashed (blue) line. All models are normalized so that the amplitudes of the growing modes at recombination are the same: $D_+(z_{rec}) = (1+z_{rec})^{-1}$, i.e., they coincide with the growth factor of the standard CDM at that redshift ($z_{rec} \approx 1090$).

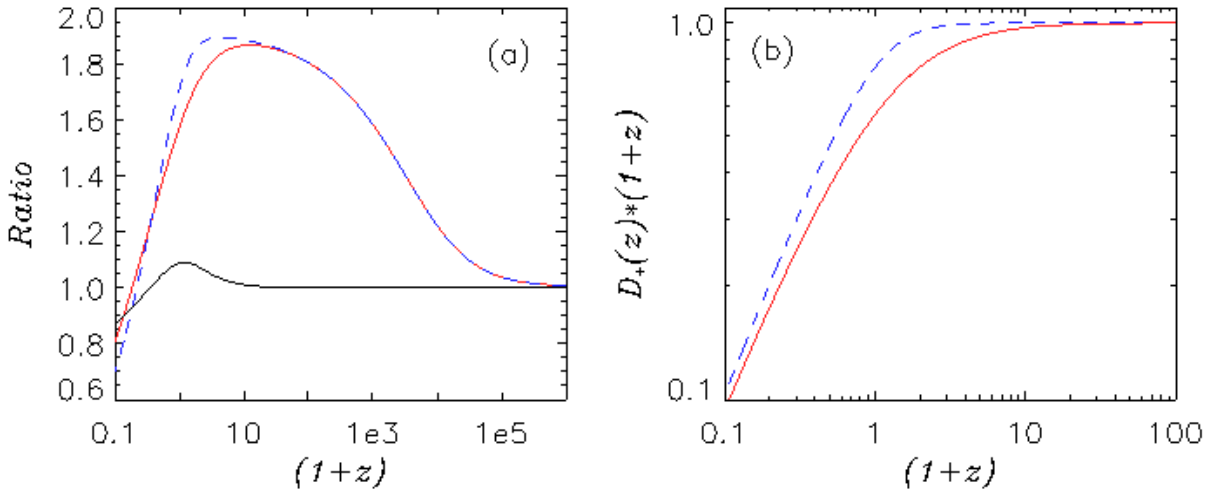

FIG. 1. (a) Ratios of the horizon radii, d_H, of three cosmological models: standard CDM, concordance ΛCDM, and the $w_{DE} = -0.5$ DE model: $d_{H,\Lambda CDM}(z)/d_{H,CDM}(z)$ (blue dashed line), $d_{H,DE}(z)/d_{H,CDM}(z)$ (thick red solid line), and $d_{H,\Lambda CDM}(z)/d_{H,DE}(z)$ (thin black solid line). (b) Growth factors of the ΛCDM (dashed blue line) and DE model (solid red line) in units of the growth factor of the standard CDM model, $D_{+,CDM} \sim (1+z)^{-1}$.

In Figures 2a,c,e we represent the exact and approximated power spectra. In each panel, the dashed black line represents the power spectra computed numerically using CMBFAST for DE with $w_{DE} = -0.8$ (a), $w_{DE} = -0.5$ (c), and $w_{DE} = -0.1$ (e). Solid (blue) lines plot the power spectra derived using our analytic approximation and dot-dashed (red) lines correspond to the concordance ΛCDM model used to construct the approximated solutions. For the first two models, the approximated and exact DE spectra are almost indistinguishable on a log-log scale. In Figures 2b,d,f we represent the ratio of the approximated to the exact (computed with CMBFAST) power spectrum (solid -blue- line) for (from top to bottom) $w_{DE} = -0.8, -0.5, -0.1$. The dot-dashed (black) line represents the ratio of the concordance ΛCDM power spectra to the exact DE power spectra. The accuracy of our prescription depends on the model parameters. It is within 1-3% for $w_{DE} = -0.8$, 1-8% for $w_{DE} = -0.5$, and degrades to 5-35% for $w_{DE} = -0.1$. Properly speaking, this latter model is not a DE model because it does not lead to a period of accelerated expansion. Even in this extreme case and ignoring the clustering of this "DE", the approximation is rather good, the largest error being 35% at $k \sim 5 \times 10^4$Mpc/h. In any case, a certain discrepancy between the numerical and approximated spectra is to be expected, as found around $k \sim 10^{-3}$Mpc/h, since for perturbations that come within the horizon after matter-radiation equality the gravitational potential is still evolving with time and Eq. (7) becomes less accurate.

Figure. 2 is our main result. It shows how useful our prescription is to construct the matter power spectrum of

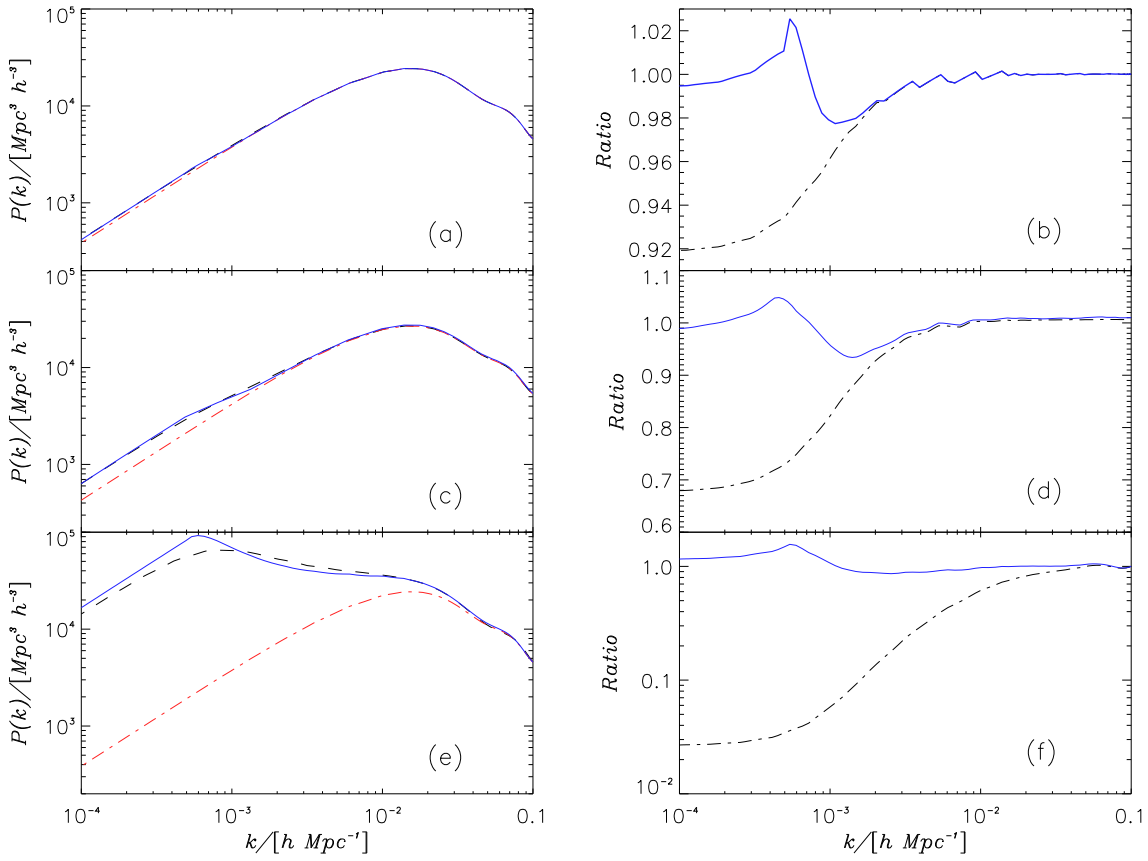

FIG. 2. (a,c,e) Matter power spectra of the concordance ΛCDM (dot-dashed red line) and the DE model (solid blue line) with EoS parameter $w_{DE} = -0.8$ (a), $w_{DE} = -0.5$ (c), and $w_{DE} = -0.1$ (e). The dashed line correspond to the numerical (CMBFAST) solution and the (blue) solid line corresponds to the approximated spectrum derived using eq. (13). All other cosmological parameters are the same as in the ΛCDM concordance model: $H_0 = 71$ km/s/Mpc, $\Omega_m = 0.27$, $\Omega_\Lambda = \Omega_{DE} = 0.73$, and $n = 1$. (b,d,f) Ratios between different matter power spectra: $P_{\Lambda CDM}(k)/P_{DE}(k)$ (dot-dashed black line), and $P_{DE,approx}(k)/P_{DE}(k)$ (solid blue line). Panel (b) corresponds to $w_{DE} = -0.8$, (d) to $w_{DE} = -0.5$, and (f) to $w_{DE} = -0.1$.

an arbitrary DE model. The closer the model parameters are to the matter power spectrum used as a starting point (in the examples above, the ΛCDM model), the more accurate the approximation is. Once the DE model parameters differ significantly, our approach is not so accurate but, at the same time, the power spectrum of the DE model separates from the concordance model. Therefore, as long as the concordance model is a good fit to the data, the difference between this model and the exact/approximated DE spectrum are so large (almost a factor 30 in the $w_{DE} = -0.1$ case) that the uncertainty of our approximation is irrelevant. Large scale structure data like CMB temperature anisotropies on large scales would certainly rule out the $w_{DE} = -0.1$ model, even allowing for a 50% uncertainty in the matter power spectrum at all scales. The $w_{DE} = -0.5$ spectrum is identical to ΛCDM at small scales, but different enough at large scales as to expect that CMB temperature anisotropies on large angular scales could rule out the model. For $w_{DE} = -0.8$, the approximate spectrum is so close to that of ΛCDM that to discriminate it from the concordance model will require background tests such as SN Ia, BAO, etc.(even if we consider the exact matter power spectrum). As determined by Larson *et al.* [18], WMAP 7yrs data alone yields $w_{DE} = -1.12^{+0.42}_{-0.43}$ at 1σ, while including data on BAO and high redshift supernova produces $w_{DE} = -0.980 \pm 0.053$ [1]. Here lies the main advantage of our approach: one can quickly construct an approximate power spectrum for any DE model that is more appealing from the theoretical point of view than the ΛCDM concordance model. When the model agrees with the data at the background level, if the matter power spectrum is very different from ΛCDM, it will not fit the observations of galaxy clustering and LSS.

IV. THE RADIATION POWER SPECTRUM

After computing the DE power spectrum, constraints on the model can be imposed using data on galaxy clustering and LSS. Since the spectral shape at small scales is the same than in the ΛCDM, once the DE model is normalized to the measured σ_8, it will reproduce the data on small scales (galaxy clustering, peculiar velocity amplitude, weak lensing convergence spectrum, etc.) as well as the ΛCDM. Of the three models discussed in Fig. 2, we shall restrict our analysis to $w_{DE} = -0.5$ DE model. As shown in Figure 1, horizon size and perturbation growth between $w_{DE} = -0.5$ DE and ΛCDM start to differ at $z \simeq 20$ and the power spectrum at $k \leq 4 \times 10^{-3} h/\mathrm{Mpc}$ (see Fig. 2c), scale that comes into the horizon well in the matter era. The differences in the matter power spectrum can only be tested using data on large scales, like CMB temperature anisotropies.

Prior to decoupling, baryon and photons are tightly coupled and inhomogeneities in the baryon distribution are also reflected in anisotropies on the radiation field. Several physical mechanisms contribute to the generation of temperature anisotropies [29]. Analytic methods that trace the structure of the cosmic microwave background anisotropies have been used to compute the contribution of different effects such as gravitational redshifts, acoustic oscillations, diffusion damping, Doppler shifts, reionization as well as the effect of curvature, a cosmological constant and their dependence on initial conditions [30]. The gravitational redshifts are the dominant contribution on large scales. These anisotropies are strongly dependent on the underlying matter power spectrum. At $l \leq 10$, the largest contributions come from the SW and ISW effects [16]. Both components can be accurately computed in terms of quadratures involving only the matter power spectrum

$$C_l^{SW} = \frac{\Omega_m^2 H_0^4}{2\pi D_+^2(0)} \int_0^\infty k^2 dk \frac{P(k)}{k^4} j_l^2(kr(z))\,, \qquad C_l^{ISW} = \frac{2}{\pi} \int_0^\infty k^2 dk P(k) I_l^2(k)\,, \tag{14}$$

where $I_l(k) = 3\Omega_{m,0} \frac{H_0^2}{c^2 k^2} \int_0^{z_{rec}} dz j_l(kr(z)) (d[(1+z)D_+]/dz)$. In these expressions j_l is the spherical Bessel function, H_0 the Hubble constant, $r(z) = \int_0^z H^{-1}(z) dz$ the look-back distance and $\Omega_{m,0}$ the current matter density in units of the critical density and D_+ is the growth factor that verifies $D_+(z) = (1+z)^{-1}$ well in the matter dominated period, so during that epoch there is no significant ISW effect. The total radiation spectrum would contain contributions such as acoustic oscillations and Doppler shifts, so $C_l \geq C_l^{SW} + C_l^{ISW}$. The accuracy of Eq. (14) could be improved by including more contributions as discussed in [32] but, as we will see below, the difference in the amplitude of the low multipoles suffices to rule out the $w_{DE} = -0.5$ DE model so the current approximation is accurate enough for our purposes.

In Fig. 3a, the thin (blue) solid and dashed lines represent the radiation spectra of the DE and ΛCDM models, respectively, computed using CMBFAST. The models are normalized to the σ_8 obtained from the code, $\sigma_8 = 0.80$ for ΛCDM and $\sigma_8 = 0.53$ for the $w_{DE} = -0.5$ DE model. The thick (red) solid line represents the power spectra computed using Eq. (14) and the dot-dashed (green) line the radiation spectra computed with the same equation but with the approximated matter power spectra. All matter power spectra are normalized to $\sigma_8 = 0.801$ [18]. The open squares correspond to the binned power spectrum measured by WMAP 7 yrs data [31]; error bars include instrumental noise and cosmic variance. To facilitate the comparison between the different approximations, the top two lines in Fig. 3b represent the ratio of the DE approximated (computed using Eq. (14) and the exact matter power spectrum) to the exact DE radiation spectrum (solid red line), and the DE (using also the approximated matter power spectrum), to the same exact DE radiation spectrum (dot-dashed green line). The dashed (black) line is the ratio of the previous two. The error introduced by computing C_l using Eq. (14) with the exact or the approximated matter power spectrum is smaller than 10%.

Fig. 3 summarizes the comparison of the $w_{DE} = -0.5$ DE model with CMB data. When CMB anisotropies are computed using CMBFAST and normalized to WMAP 7 yrs data, the CMB power spectrum fits the low multipoles rather well, but then the amplitude of matter density fluctuations is $\sigma_{8,DE} = 0.53$, well outside the value $\sigma_8 = 0.801 \pm 0.030$ [18] allowed by the data. As a result, the $w_{DE} = -0.5$ DE model with parameters $\Omega_m = 0.27$, $\Omega_\Lambda = 0.73$, etc. is ruled out. But if the calculation of the CMB power spectrum proves to be difficult, the approximated power spectrum could be used to approach the problem differently. Once the power spectrum of the DE model (with $w_{DE} = -0.5$) is constructed and normalized to $\sigma_8 = 0.801$, the amplitude of temperature anisotropies at $l \leq 10$ would result $l(l+1)C_l^{DE}/2\pi \sim 2000(\mu K)^2$, about a factor of 2 larger than the measured spectrum, a factor larger than the uncertainties introduced by our approximation (less than 10%) or by Eq. (14) (less than 15% for $l \leq 10$). Therefore, without the need of further information, a model like DE with $w_{DE} = -0.5$ could be ruled out based on the amplitude of the low order multipoles. Models that differ

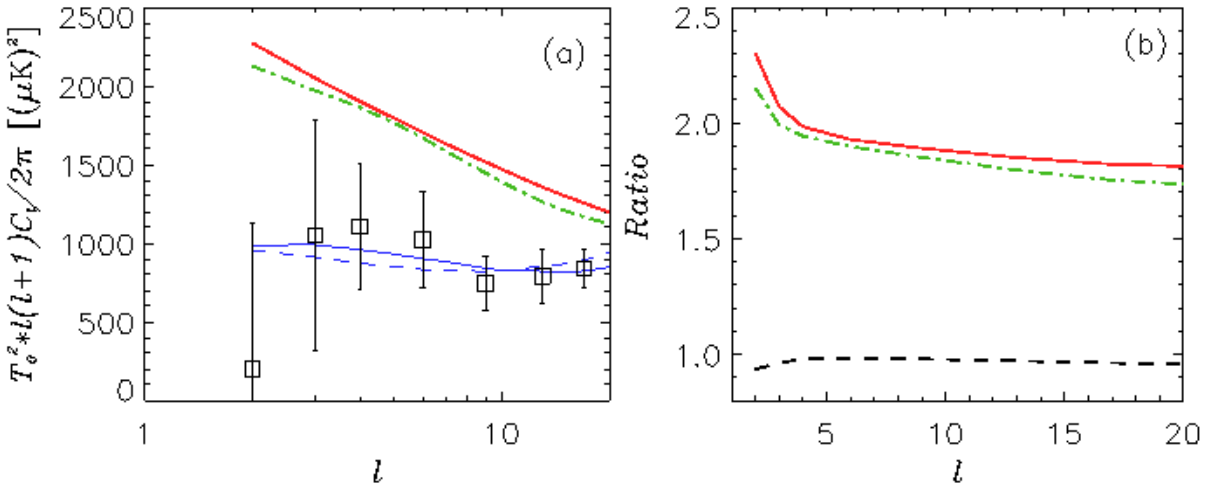

FIG. 3. (a) Power spectra of the CMB temperature anisotropies. Thin dashed (blue) and solid (blue) lines represent the exact spectrum of the ΛCDM model (with $\sigma_8 = 0.801$) and DE model ($\sigma_8 = 0.53$), respectively. Thick (red) solid and dot-dashed (green) lines plot multipoles computed using eq. (14) with the exact and approximated matter power spectrum, both normalized to $\sigma_8 = 0.801$. The data are WMAP 7yrs measurements. (b) $C_{l,DE,eq\ 14}/C_{l,DE,CMBFAST}$ using eq. (14) and the exact and approximated matter spectra, solid (red) and dot-dashed (green) lines respectively. The dashed (black) line represents the ratio of the previous two.

from ΛCDM also during the radiation regime can be more severely constrained by using weak lensing, peculiar velocities, or galaxy clustering data.

V. CONCLUSIONS

We have shown how to compute the matter power spectrum of DE cosmological models using a fiducial ΛCDM model and the growth factor of subhorizon density perturbations of the model under consideration. This allows to use data on CMB temperature anisotropies and galaxy clustering to discriminate models without having to solve the evolution of density perturbations of all matter components, thus economizing much effort. Figure 2 shows the advantage of our proposal. In most cosmological models, the equations describing the time evolution of matter density perturbations can be derived from the conservation of the energy momentum tensor and solved for each component individually. Thus, an approximated matter power spectrum can be easily computed. If a model fits the background evolution as determined, for example, by luminosity distances obtained from supernovae data, before proceeding to a detailed study of the evolution of its density perturbations and CMB anisotropies, one can compute an approximated matter power spectrum and predict observables such as the low multipoles of the CMB, the ISW-LSS correlation, the weak lensing convergence spectrum, etc., that can be compared with observations. Even if a model agrees with the data on the expansion rate of the Universe, it could be ruled out by data on temperature anisotropies or galaxy clustering without requiring to solve the first order perturbation equations in full.

Our method has its limitations: it produces an approximated matter power spectrum and only observables derived from it can be used. Since it fixes amplitudes at horizon crossing, it is insensitive to any instability that could occur on superhorizon scales such as those present in some models with DM/DE interactions [33]. However, as our examples show, the approximated and numerical power spectra are very similar when the model parameters are close to those of the starting model. This is the advantage of our approach: the approximated power spectrum can be used to distinguishing models, that despite reproducing the background observational data, would fail to fit the galaxy clustering and LSS data. In this respect, the $w_{DE} = -0.8$ model is so close

to ΛCDM it should be tested with background data such as SN Ia, BAO etc. to be ruled out (the same happens with the exact matter power spectrum). In the $w_{DE} = -0.5$ DE model, the relative error in the approximated and numerical $P(k)$ is smaller than 8%, but the difference with the concordance model is so significant that the predicted CMB temperature anisotropies on large scales are about a factor of 2 larger than the measurements, a factor much larger than the uncertainty introduced by our approximation or by Eq. (14). Finally, the $w_{DE} = -0.1$ is so different from ΛCDM that it can be ruled out at a glance, irrespectively of the poorer quality of our approximation. When the observables derived from the approximated matter power spectrum fails to fit the data, we can confidently expect the model to fail. But even if a model fits some data on galaxy clustering, it may not necessarily reproduce all the observations, like the full spectrum of CMB temperature anisotropies; it simply means that it deserves further study.

ACKNOWLEDGMENTS

The research of I.D. and D.P. was partially supported by the "Ministerio Español de Educación y Ciencia" under Grant No. FIS2009-13370-C02-01 and by the "Direcció de Recerca de la Generalitat" under Grant Number 2009SGR-00164. I.D. was funded by the "Univesitat Autònoma de Barcelona" through a PIF fellowship. F.A-B. acknowledges financial support from the spanish Ministerio de "Educación y Ciencia", Grants No. FIS2009-07238 and CSD 2007-00050.

[1] E. Komatsu *et al.*, Astrophysical J. Supplement Series 192, 18 (2011).
[2] A.R Liddle, Monthly Not. R. Astron. Soc. 351, L49 (2004).
[3] L. Amendola, M. Quartin, S. Tsujikawa, I. Waga, Phys. Rev. D 74, 023525 (2006).
[4] S. Weinberg, Rev. Modern. Phys. 61, 1 (1989).
[5] P.J. Steinhardt, in *Critical Problems in Physics*, edited by V.L. Ficht and D.R. Marlow (Princeton University Press, Princeton, 1997).
[6] J.A. Friemann, M.S. Turner and D. Huterer, Ann. Rev. Astron. Astrophys. 46, 385 (2008); R. Durrer and R. Maartens, Gen. Relativ. Grav. 40, 301 (2008); R.R. Caldwell and M. Kamionkowski, Ann. Rev. Nucl. Part. Sci. 59, 397 (2009); L. Amendola and Tsujikawa, *Dark Energy. Theory and Observations* (CUP, Cambridge, 2010).
[7] P.J.E. Peebles, B. Ratra, 2003, Rev. Mod. Phys. 75, 559; F. Atrio-Barandela and D. Pavón in "Dark Energy: Current Advances and Ideas", Jeong R. Choi Ed., Research Signpost, Kerala (India), p51 (2009).
[8] C. Wetterich, Astron. Astrophys. 301, 321 (1995); C. Wetterich, Nucl. Phys. B 302, 668 (1988); G. Olivares, F. Atrio-Barandela, and D. Pavón, Phys. Rev. D 71, 063523 (2005); G. Olivares, F. Atrio-Barandela, and D. Pavón, Phys. Rev. D 74, 043521 (2006).
[9] R. Lazkoz, and E. Majerotto, JCAP 07, 15 (2007); C.G. Böhmer, G. Caldera-Cabral, R. Lazkoz, and R. Maartens, Phys. Rev. D 78, 023505 (2008); J. Beltrán Jiménez, R. Lazkoz, and A.L. Maroto, Phys. Rev. D 80, 023004 (2009).
[10] I. Duran, D. Pavón, and W. Zimdahl, JCAP 07, 018 (2010); I. Duran, and D. Pavón, Phys. Rev. D 83, 023504 (2011).
[11] G. Olivares, F. Atrio-Barandela, and D. Pavón, Phys. Rev. D 77, 063513 (2008);
G. Olivares, F. Atrio-Barandela, and D. Pavón, Phys. Rev. D 77, 103520 (2008);
J.-H. He, B. Wang, and Y. P. Jing, JCAP 07, 030 (2009);
X.-D. Xu, J.-H. He, and B. Wang, Phys. Lett. B 701, 513 (2011);
J.-H. He, B. Wang, and E. Abdalla, Phys. Rev. D 83, 063515 (2011).
[12] H-C Kao, W-L Lee, and F-L Lin, Phys. Rev. D 71, 123518 (2005);
D. Rowland and I.B. Whittingham, Mon. Not. R. Astron. Soc. 390, 1719 (2008);
E.M. Barboza Jr. and J.S. Alacaniz, Phys. Lett. B 666, 415 (2008);
L. Amendola, M. Baldi, and C. Wetterich, Phys. Rev. D 78, 023015 (2008);
M. Li, X-D Li, S. Wang, Y. Wang, and X. Zhang, JCAP 12, 014 (2009);
Y. Chen, Z-H Zhu, L. Xu and J.S. Alcaniz, Phys. Lett. B 698, 175 (2011);
S. del Campo, J.C. Fabris, R. Herrera, and W. Zimdahl, Phys. Rev. D 83, 123006 (2011);
L.P. Chimento, M. Forte, and M.G. Richarte, arXiv:1106.0781 (2011).
[13] A. Kashlinsky, and B.J.T. Jones, Nature 349, 753 (1991).
[14] M. Strauss, and J. Willick, Phys. Rep. 261, 271 (1995).
[15] B. M. Schaefer, G. A. Caldera-Cabral, and R. Maartens (2008), 0803.2154.
[16] R.K. Sachs, and A.M. Wolfe, Astrophys. J. 147, 73 (1967).

[17] R.G. Crittenden and N. Turok, Phys. Rev. Lett. 76, 575 (1996);
A. Cooray, Phys. Rev. D 65, 103510 (2002).
[18] D. Larson *et al.*, Astrophys. J. Supplement Series 192, 16 (2011).
[19] A. Kashlinsky, F. Atrio-Barandela, D. Kovecski, H. Ebeling, Astrophys. J. 686, L49 (2008);
R. Watkins, H.A. Feldman, M.J. Hudson, Mon. Not. R. Astron. Soc. 392, 743 (2009);
A. Kashlinsky, F. Atrio-Barandela, H. Ebeling, A. Edge, D. Kovecski, Astrophys. J. 712, L81 (2010);
A. Kashlinsky, F. Atrio-Barandela, H. Ebeling, Astrophys. J. 732, 1 (2011);
J. Colin, R. Mohayaee, S. Sarkar, A. Shafieloo, Mon. Not. R. Astron. Soc, 414, 264 (2011);
S.J. Turnbull *et al.*, Mon. Not. R. Astron. Soc. (in press), arXiv:1111.0631 (2011).
[20] G. Olivares, F. Atrio-Barandela and D. Pavón, Phys. Rev. D 77, 103520 (2008);
R. Kimura, T. Kobayashi and K. Yamamoto, arXiv:1110.3598 (2001).
[21] E.R. Harrison, Phys. Rev. D 1, 2726 (1970);
Ya.B. Zeldovich, Mon. Not. R. Astron. Soc. 160, 1 (1972).
[22] U. Seljak, and M. Zaldarriaga, Astrophys. J. 469, 437 (1996);
U. Seljak, M. Zaldarriaga, and E. Bertschinger, Astrophys. J. 494, 491 (1998);
M. Zaldarriaga, and U. Seljak, Astrophys. J. Supplement Series 129, 431 (2000);
http://lambda.gsfc.nasa.gov/toolbox/tb_cmbfast_ov.cfm.
[23] L. P. Chimento, A. S. Jakubi, D. Pavón and W. Zimdahl, Phys. Rev. D 67, 083513 (2003);
[24] B. Wang, Y. Gong and E. Abdalla, Phys. Lett. B 624, 141 (2005).
[25] D. Pavón and W. Zimdahl, Phys. Lett. B 628, 206 (2005).
[26] H. Kodama, and M. Sasaki, Progress of Theoretical Physics Supplement 78, 1 (1984);
V.F. Mukhanov, H.A. Feldman, and R.H. Brandenberger, Phys. Rep. 215, 203 (1992);
C.-P. Ma, and E. Bertschinger, Astrophys. J. 455, 7 (1995).
[27] G. Caldera-Cabral, R. Maartens, and B.M. Schaefer, JCAP 07, 027 (2009).
[28] L. Wang and P. J. Steinhardt, Astrophys. J. 508, 483 (1998).
[29] W. Hu, N. Sugiyama, and J. Silk, Nature 386, 37 (1997).
[30] W. Hu, and N. Sugiyama, Astrophys. J. 444, 489 (1995);
W. Hu, and N. Sugiyama, Phys. Rev. D 51, 2599 (1995).
[31] The data can be downloaded from http://lambda.gsfc.nasa.gov/.
[32] F. Atrio-Barandela, and A. Doroshkevich, A. Klypin, Astrophys. J. 378, 1 (1991);
F. Atrio-Barandela, and A. Doroshkevich, Astrophys. J. 420, 26 (1994);
A.G. Doroshkevich, and R. Schneider, Astrophys. J. 469, 445 (1996);
V. Mukhanov, Int. J. Theoretical Phys., 43, 623 (2004).
[33] H. B. Sandvik, M. Tegmark, M. Zaldarriaga and I. Waga, Phys. Rev. D 69, 123524 (2004);
J. Valiviita, E. Majerotto, and R. Maartens, JCAP 07, 020 (2008).